A simple and robust approach for visual overload indication - UD thin-ply hybrid composite sensors

Tamas Rev[1*], Meisam Jalalvand[2], Jonathan Fuller[3], Michael R. Wisnom[1], Gergely Czél[4,1]

[1]Bristol Composites Institute (ACCIS), University of Bristol, Queen's Building, BS8 1TR, Bristol, United Kingdom

[2]Department of Mechanical and Aerospace Engineering, University of Strathclyde, 75 Montrose Street, G11XJ, Glasgow, UK

[3]National Composites Centre (NCC), Bristol & Bath Science Park, Emersons Green, BS167FS, Bristol, UK

[4]Department of Polymer Technology, Budapest University of Technology and Economics, Műegyetem rkp. 3., H-1111 Budapest, Hungary

*corresponding author, e-mail: tamas.rev@bristol.ac.uk

Abstract

A novel, purpose-designed, thin interlayer glass/carbon-epoxy hybrid composite sensor concept is presented here that can be used for structural health monitoring (SHM), offering potential for safer operation in service. The hybrid composite sensors indicate the overload of a structure by exhibiting a change in their appearance when loaded in tension over a predefined strain value. The sensors can be attached to a component either as a structural sensing layer or integrated locally as demonstrated in this study through real-life applications. Furthermore, various test methods have been utilised to characterise the bonded-on sensors including mechanical testing, Digital Image Correlation (DIC) and Acoustic Emission (AE) measurements. An optimal configuration has been identified with the utilised materials that

can potentially be used in applications such as sporting goods, civil engineering structures (e.g. truss and bridge elements) as well as pressure vessels.

Keywords:

Hybrid; Fragmentation; Delamination; Failure; Mechanical Testing;

1. Introduction

Fibre reinforced composite materials are increasingly used in advanced lightweight applications as forecasted earlier [1], especially in the aerospace and space sector as well as automotive, civil engineering [2] and high-end sports industries [3,4]. Since the performance of engineering materials in service is usually different to what is expected of them, engineers are usually obliged to design structures and components to minimize the possibility of failure [5].

In high volume applications such as the automotive industry or civil engineering, it is of immense importance to ensure an appropriate safety margin as a sudden failure or collapse could lead to the loss of human life as well as significant financial costs. In these areas, the scope of composite applications is hindered as sudden failure and poor residual load bearing capacity cannot be tolerated. Instead, higher safety margins and conservative design envelopes have become the standard practice in composites design and manufacture. Another issue with engineering materials is that failure may occur without preceding detectable damage or warning of any kind especially for composite materials [6,7].

Structures that pass visual inspection can fail at much lower loads than expected [8] hence it is crucial to monitor their integrity as well as detect damage (if there is any) before final failure occurs. As a result, damage detected in time can not only prevent sudden, catastrophic failure but it can also indicate the need for further, more thorough non-destructive testing (NDT) so appropriate repair or maintenance can be carried out when necessary, leading to no unexpected down-time and enhanced service lives.

The process of monitoring damage during service life is often referred to as Structural Health Monitoring (SHM). It is very common, especially in civil engineering and transportation applications where sensors based on different principles - such as fibre optics, piezoelectrics, magnetostricity, and self-sensing - are used in order to assess the integrity or certain physical or chemical properties of a structure or component. An extensive review on SHM techniques as applied to composite structures can be found in the study by Amafabia et al. [9]. In general, a structural health monitoring system comprises three different constituents: the sensor itself that is coupled with the monitored structure, as well as a data acquisition and a data evaluation system [10,11].

For the health monitoring of civil structures, fibre optic sensors (FOS), particularly Fibre Bragg Grating (FBG) sensors have been often used to mitigate the risk of unexpected failure. Especially for composite materials that are prone to failure due to an overload or an impact event, these lightweight sensors can be utilised at various locations without affecting the performance of the structure [10,12]. A drawback of such sensors is that they require equipment to detect the signals and process data.

Fibre optic sensors are insensitive to electromagnetic interference (EMI) and sense various parameters such as strain or displacement. Even though they are brittle, and need to be encapsulated in a protective material, they are extensively used in civil applications such as bridges, tunnels, pipelines and in a currently expanding field: wind turbine blades [11] as discussed in a comprehensive review on optical fibre sensing technologies by Ye et al [13].

Another emerging technology for SHM is the field of self-sensing composites. These multi-functional materials are able to indicate their own physical conditions such as stress, strain or temperature as well as deformation and damage [10]. E.g. a change in electrical conductivity is used for monitoring damage as it can be directly related to fibre breakage [14]. In a similar way, various other damage mechanisms e. g. delamination [15] and matrix cracking

[16], under different loading conditions [17–19], have been investigated. These measurements are based on a piezoresistive principle: incorporating a conducting element e. g. carbon particles, nanomaterials (carbon nanofibres and carbon nanotubes [20]) or short or continuous carbon fibres [10,21,22] that form a 'sensing' network in the composite. When the composite is subjected to an overload or deformation, this network is disturbed, hence changing the electrical resistivity of the overall structure.

Previously, when demonstrating pseudo-ductile behaviour in thin interlayer glass/carbon-epoxy hybrid composites, a pattern was observed by Czél and Wisnom [8] during the gradual failure of the specimens. The translucent nature of the constituent glass-epoxy layers made delamination detection possible to the naked eye. It was realised that this can be used for sensing damage on the surface of a structure hence this paper introduces the hybrid composite sensor concept developed by Czél et al. [23] that can be used for SHM purposes in composite or other structures, offering potential for safer operation in service.

Various other authors have tried to combine the advantageous pseudo-ductile behaviour achieved by fibre hybridisation with the functionality of self-sensing. Bakis et al. [24] demonstrated pseudo-ductile tensile behaviour with the capability of monitoring strain and damage by the hybridization of low-strain piezoresistive carbon fibres and high-strain non-conductive fibres. Nanni et al. [25] have designed a system consisting of a carbon-glass hybrid structure that offers good structural properties while acting as a warning signal when reaching certain loading conditions. In both studies, the sensors are based on a piezoresistive principle while being low-cost, versatile and easy to fabricate. The sensors proposed here indicate an overload by simply exhibiting a change in appearance in contrast with other strain sensors that are based for example on the change of electrical properties induced by deformation.

They are robust and lightweight, completely wireless, and do not require any data acquisition or evaluation system hence offering a low-cost and simple visual solution for strain

overload indication. This novel concept can be simultaneously used for SHM and structural load-carrying purposes. The hybrid composite sensors can either be a sensing layer as part of the structure or can be bonded on to the surface of composite or metallic structures. They can provide more information about the magnitude of the overload by combining various sensing materials indicating different strains. They can also provide information on the direction of overload by applying an array of sensors integrated in different directions.

The aim of this paper is to introduce this novel strain overload indication technology and to demonstrate the proof of concept for the bonded-on sensors on a real-life structural application. Some preliminary results were presented before, mainly to investigate stiffness effects and the accuracy of the sensors [26]. In this paper we present an extended assessment of the concept. To bridge the gap between the concept and an actual application, characterisation and validation of basic sensor configurations have been carried out using available measurement techniques such as a videogauge, strain gauges and digital image correlation (DIC) in order to assess the strain in the substrate and the sensor during uniaxial tensile loading. Furthermore, it has been shown that these new UD hybrid sensors can be integrated into the substrate material. A commercially available CFRP bike handlebar has been fitted with bonded overload sensors and tested to demonstrate the novel sensing concept.

2. Sensing mechanism

This section gives a brief summary on the principle behind the unidirectional hybrid composite sensor concept as well as the underlying mechanism that enables the visual overload indication.

2.1. Failure mechanism

The damage and failure mechanism leading to visual strain overload indication is based on the hybridisation approach of UD glass/epoxy and thin carbon/epoxy plies to create interlayer hybrid composites [8].

As has been reported, well-designed thin ply-hybrids can develop multiple fractures of the higher modulus/lower strain constituent (fragmentation) avoiding catastrophic failure and unstable delamination due to the low energy release rate that depends primarily on the thickness of the stiffer component layer in the hybrid [8]. The observed carbon ply cracks and delamination are clearly visible to the naked eye due to translucency of the glass/epoxy plies. They appear along the gauge length of tensile specimens in a well-dispersed, striped pattern [6,8]. The aforementioned fragmentation of the low strain material followed by gradual, dispersed delamination [6] is illustrated in Figure 1 (a).

Figure 1 (b) represents another pattern type and failure mechanism for thicker carbon layers: a single fracture of the low strain material followed by sudden, unstable delamination [27], where the fracture of the stiffer layer translates to a significant stress drop at the corresponding strain to failure of the low strain material on the stress-strain curves. While the latter one gives a clearer indication of an overload event as it is easier to observe the delamination through the translucent glass layer, the former mechanism (studied and used in this paper) with multiple fragmentation and decreasing spacing between cracks allows for a quantitative indication on the severity of the overload event.

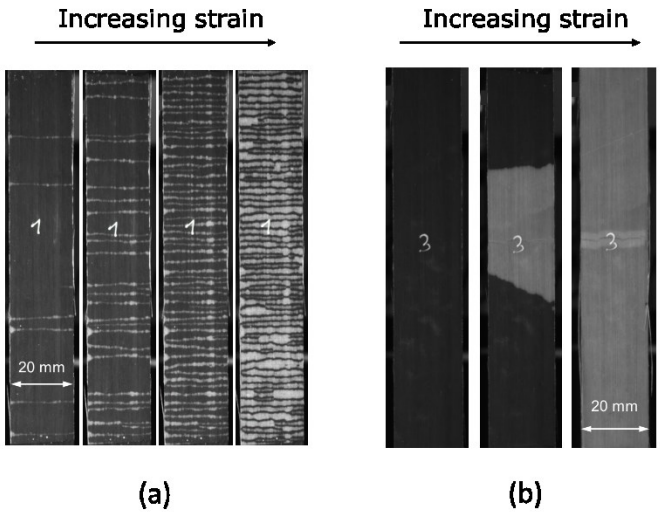

Figure 1. Visual patterns based on different failure mechanisms of thin-ply glass/carbon hybrids: (a) carbon layer fragmentation followed by stable, dispersed delamination [6] (b) carbon layer fracture followed by sudden delamination [27]

2.2. Principle – change of appearance

The principle behind the UD hybrid sensor concept is based on a unique feature of the aforementioned purpose-designed thin interlayer glass/carbon hybrid composites: the change in their appearance when loaded beyond a predefined strain. The sensor is on the surface of the component, and experiences similar strains as the material beneath. It consists of a 'sensing' layer and an outermost layer, which in this case are a carbon sensing layer and glass outermost layer respectively. The schematic of the sensor-set up and its attachment to a substrate material is illustrated in Figure 2.

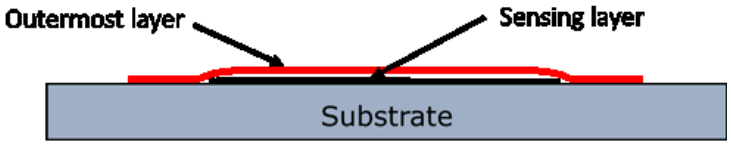

Figure 2. Schematic of a hybrid composite strain overload sensor attached to a substrate material

The originally intact carbon layer absorbs the incident light through the translucent glass layer showing a dark appearance as seen in Figure 3 (a). After the strain exceeds the failure strain of the carbon layer, the carbon layer develops multiple fractures and the incident light is reflected back from the locally damaged glass/carbon interface around the carbon layer fractures, exhibiting light stripes as illustrated in Figure 3 (b). The visible interfacial damage is caused by the fragmentation of the carbon fibre sensing layer followed by stable, dispersed delamination as previously presented by Czél et al [6].

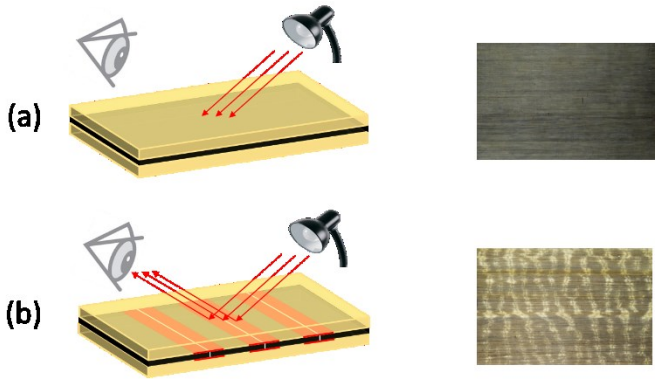

Figure 3. The sensing mechanism behind the hybrid composite strain overload sensors: (a) intact carbon layer absorbing light at glass/carbon interface (b) striped pattern visible due to light being reflected from locally damaged glass/carbon interface around the sensing layer cracks.

3. Materials and configuration design

3.1. Choices in design, manufacture and sensor integration

There are various parameters influencing the design of the proposed hybrid composite sensors. Their geometry (length and width) can be varied as well as the stiffness ratio of the sensor to the substrate by either changing the thickness of the layers or by utilising different composite prepreg materials. The most important parameter is the sensors' trigger strain that is controlled by the failure strain of the carbon fibre sensing layer. The integration of the sensors can be achieved by either co-curing or retrofitting by bonding onto finished parts. By co-

curing on the surface, the sensor will act as a structural sensing layer while by retrofitting it will act as a discrete sensor on the structure. Furthermore, the sensors can indicate both the magnitude of the overload strain (pre-defined by the sensing layer material) and the direction of a given overload strain if multiple sensors are utilised in various directions. The material system proposed in this study is suitable for the fabrication of sensors designed for tensile load dominated applications, although fragmentation in thin ply hybrids has also been reported in compression [27].

3.2. Materials

There is a wide range of materials that can be used for demonstrating the concept explained above, however two criteria must be considered: (i) in order to apply such composite sensors, the strain to failure of the 'sensing' carbon fibres has to be considered according to the surface strain of the material underneath and (ii) the thickness of the sensing material has to be thin enough to exhibit failure with fragmentation and dispersed delamination. The applicable strain range currently for carbon fibre materials satisfying these conditions is from 0.3% - 2%, however it can be extended by using a wider range of materials.

The material considered as an outermost, translucent layer was a standard thickness UD S-glass/epoxy prepreg supplied by Hexcel. The sensing layer was thin UD XN80/epoxy carbon prepreg produced by North Thin Ply Technology (NTPT). For the demonstration of the sensors, a substrate material of IM6 carbon fibre reinforced epoxy prepreg supplied by Cytec has been used. The resin systems used for the sensor and substrate have a similar cure temperature, hence suitable for curing together in the autoclave. The basic material data of the applied fibres and prepreg systems can be found in Table 1 and Table 2.

Table 1. Fibre properties of the applied unidirectional prepregs based on manufacturers data (carbon fibre types: IM – intermediate modulus, UHM – ultra high modulus)

Fibre type	Manufacturer	Elastic modulus [GPa]	Density [g/cm^3]	Strain to failure [%]	Tensile strength [GPa]
Granoc XN80	Nippon GFC	780 (UHM)	2.17	0.5	3.43
Hextow IM6	Hexcel	279 (IM)	1.76	1.9	5.72
FliteStrand S ZT S-glass	Owens corning	88	2.45	5.5	4.8-5.1

Table 2. Cured ply properties of the applied unidirectional prepregs

Prepreg type	Areal density[1] [g/m^2]	Cured ply thickness[2] [μm]	Fibre volume fraction[2] [%]	Initial elastic modulus[2] [GPa]	Tensile strain to failure [%]
XN80/thinpreg carbon/epoxy	63	63	46.5	364.4	0.5[3]
IM6/950 carbon/epoxy	135	153	50	141.2	1.8[2]
S-glass/913 glass/epoxy	190	155	51	45.6	3.9[3]

[1]Based on manufacturer's data
[2]Calculated using manufacturer's data
[3]Based on measurements

Additional adhesives were utilised for the fabrication of specimens with retrofitted sensors: including an Araldite 2014/1 type two-part epoxy adhesive (Huntsman), 913 resin film (Hexcel), a commercially available Permabond cyanoacrylate adhesive, and an M-Bond AE-15 two-part high-elongation adhesive system (Vishay) developed for the application of strain gauges.

4. Experimental

4.1. Sensor response and accuracy

One of the key design parameters influencing the sensing behaviour of such hybrid composites is the critical or ineffective length of the layer. Sensing layers shorter than the ineffective length are not capable of reaching the fibre fracture strain, hence rendering them unable to function properly. The assumed stress distribution along the length of the sensing layer(s) is illustrated in Figure 4.

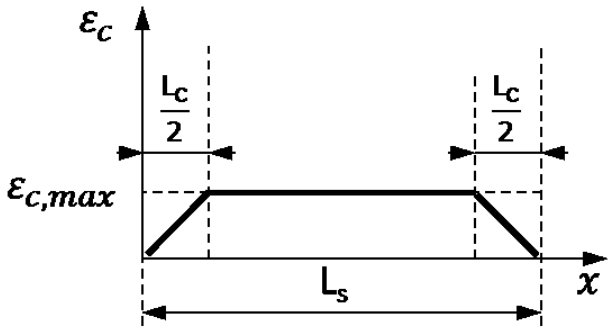

Figure 4. Strain distribution in the sensing layer along its length (L_s) at trigger strain (if $\varepsilon_c = \varepsilon_{c,max}$)

Calculations have been carried out to estimate the critical length L_c of the different thickness carbon/epoxy sensing layer. The formulation and the mechanical background is similar to the Kelly-Tyson equation applied at the ply rather than fibre/matrix level as given in equation (1) [28]:

$$L_c = \frac{E_c \ \varepsilon_{cmax} \ t_c}{\tau_{max}} \tag{1}$$

, where E_c is the Young modulus of the sensing carbon layer, $\varepsilon_{c\,max}$ is the strain to failure of the carbon layer, t_c is the thickness of the sensing layer and τ_{max} is the interfacial shear strength at the glass/carbon layer interface. τ_{max} is assumed to be 100 MPa based on test results of the

same resin system used in [29]. This equation is based on the assumption that there are two active interfaces transferring load to the layer under investigation.

The critical length L_c is required to assess the transfer of tensile stresses (from the substrate) through shear to the specific layers of the sensor. This ineffective length is strongly dependent on the stiffness of the constituent sensor layers. The calculated values for the constituent layers are illustrated in Table 3.

Table 3. Calculated critical length values for the carbon constituent layer(s) with different incorporated sensing plies

	$XN80_2$	XN80
Critical length [mm]	4.87	2.44

Another key parameter to consider when designing such sensors is the sensor to substrate stiffness ratio as explained in [26]. It is important to determine how much the stiffness of the substrate is affected by the sensor. Simple calculations can be carried out with respect to the axial stiffness of the sensor and substrate to check the stiffness increment caused by the sensors. Building on that, a simple analytical model developed by the authors [26] allows for an assessment of whether a calibration is necessary to account for this effect. In general, the lowest stiffness sensors on high stiffness substrates provide the most accurate results by not increasing the substrate stiffness significantly. It has to be noted that accuracy in this case represents the percentage error between the substrate strain and the sensor strain. In practice, the sensors have to be made the thinnest and narrowest possible if the substrate has a relatively low stiffness.

4.2. Manufacturing

All composite laminates have been fabricated by the conventional process that is used for prepreg composite manufacturing. Following hand lay-up, a standard bagging method was applied on a flat aluminium tool plate. Additional silicone sheets were placed on top of the laminates in order to ensure a smooth top surface and an even pressure distribution in the autoclave.

The laminates were then cured in an autoclave at the recommended temperature and pressure cycle. As different material combinations were used, the highest cure temperature and longest curing time of all the constituent prepregs' individual cure cycles have been used to ensure full cure for all the prepreg systems and to obtain the desired mechanical performance. The curing cycle used for the co-cured plates - consisting of the substrate laminate and the hybrid sensor layers - as well as for the substrate plates cured on their own was 155 mins@137 °C, with 0.7 MPa applied pressure and a ramp up rate of 2°C/min. In this material combination, the 137 °C peak temperature is due to the IM6/950 material's curing cycle being 135 °C with an additional 2 °C overrun. The cycle used for the sensor laminates to be retrofitted was 165 mins@127 °C, with 0.7 MPa applied pressure and a temperature ramp up rate of 2°C/min. The 127 °C peak temperature in this case reflects the highest 125 °C cure temperature for the S-Glass/913 material, also with an additional 2 °C overrun.

All the tensile coupons were fabricated by using a diamond cutting wheel. Untapered, 1.7 mm thick end-tabs made of a balanced woven glass fibre fabric reinforced composite laminate were bonded to the specimens using an Araldite 2014/1 type epoxy adhesive system. The samples were then put into an atmospheric oven to cure the adhesive for 120 mins@80 °C.

Regarding the separately manufactured sensor laminates to be retrofitted, sensor strips were cut to the desired width and their surfaces were roughened with coarse sandpaper before attachment to the substrate/component.

Various adhesives and methods have been utilised for bonding the sensors to the substrates. The two fabrication techniques included simple mechanical clamping and vacuum-assisted envelope bagging to ensure an adequate pressure while curing the adhesives. Both fabrication methods have been applied using the three previously mentioned adhesives, giving a total of 6 differently bonded retrofitted specimen types.

4.3. Specimen configuration and geometry

All sensors consist of one or two layers of XN80/epoxy and one layer of S-glass/epoxy prepreg material. The schematic of the specimens both co-cured and separately manufactured sensor strips are illustrated in Figure 5 (a) and (b) respectively.

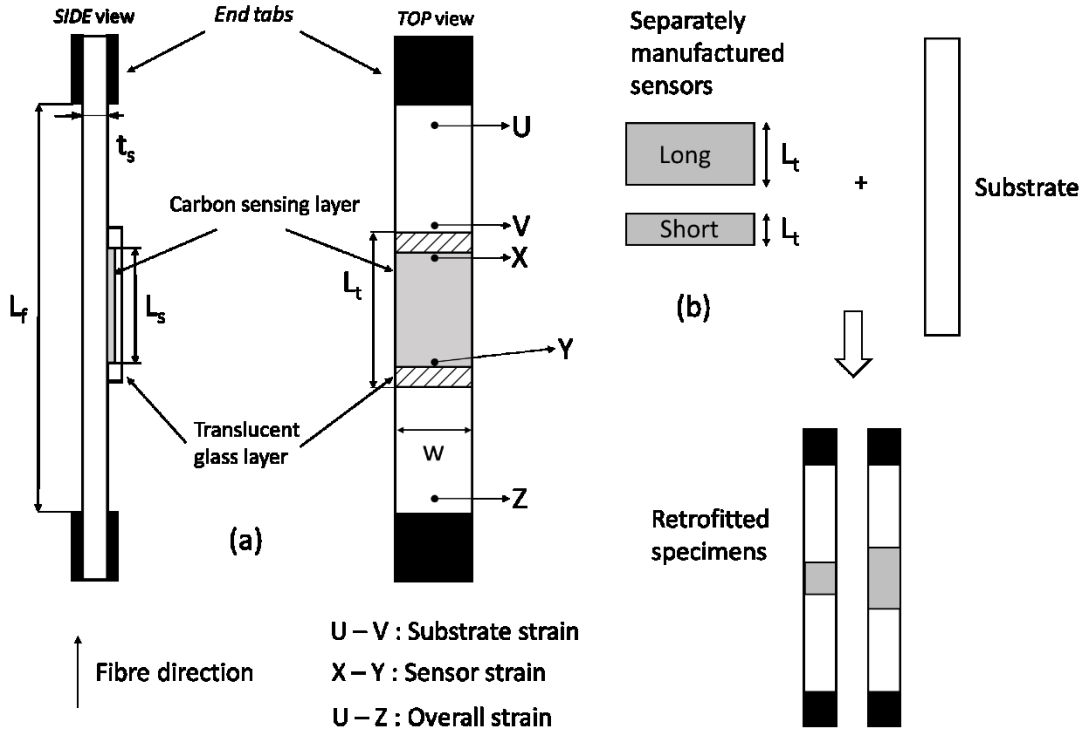

Figure 5. An illustration of (a) a unidirectional tensile specimen equipped with hybrid composite strain sensor (b) separately manufactured sensor strips for retrofitting purposes

The nominal specimen dimensions were 260/160/20/2.4 mm overall length/free length (L_f) /width (w)/thickness (t_s) respectively while nominal sensor dimensions were 50/30

mm (long sensor) and 20/10 mm (short sensor) total length (L_t)/sensor length (L_s) respectively. The substrate laminates comprised 15 plies of unidirectional IM6 carbon/epoxy prepreg.

The co-cured specimens were fabricated with long, single and double layer XN80/epoxy sensor laminates in the central section on one side to investigate the effect of having a range of stiffnesses added to the structure. The effect of the different integration methods was investigated by fabricating specimens with both co-cured and retrofitted sensors. After initial testing it was found that the single layer XN80/epoxy sensors worked satisfactorily and visually indicated the overload of the substrate. Therefore, the retrofitted specimens were fabricated with only single layer XN80/epoxy sensing layers. The retrofitted specimens were also equipped with both long and shorter length sensors to investigate the effect of sensing layer length on the sensor trigger strain. The curved sensors for the bike handlebar demonstrators were fabricated using both longer and shorter sensor geometries as well as various widths depending on the geometry of the component they are designed for. A summary illustrating the various configurations can be found in Table 4.

Table 4. Summary of the fabricated configurations

	Double layer sensor	Single layer sensor	Long sensor	Short sensor
Co-cured specimens	✓	✓	✓	
Retrofitted specimens		✓	✓	✓
Demonstrator application		✓	✓	✓

4.4. Test methods

Mechanical testing of both co-cured and retrofitted specimens was carried out on an INSTRON 8801 100 kN rated, computer controlled, universal servo-hydraulic test machine

with wedge type hydraulic grips under uniaxial tensile loading and displacement control at a crosshead speed of 1 mm/min. The clamping pressure was kept high enough to avoid slippage of the specimens in the grips. Various local (sensor) and global strains (see Figure 5) were measured using an Imetrum videogauge system, with the test machine outputting the corresponding force signals. The high-definition extensometer videos recorded during the tests were kept mainly for determining the first fracture of the carbon sensing layer by visual inspection.

Another optical analysis method, Digital Image Correlation (DIC) was also used in order to determine the strain distribution of the optimal co-cured specimens fitted with single layer XN80/epoxy sensors. The specifications and parameters for the DaVis DIC measurement system are summarised in Table 5.

Table 5. DIC measurement specifications

Technique	Stereo DIC
Software	LaVision DaVis 8.3.1
Subset Size [pixels]	29
Step Size [pixels]	10
Camera	VC-Imager 16MPixel
Lens	Tokina ATX AF 100/2.8
Resolution [pixels]	3404 x 4800
Field of view [mm]	101.4 x 66.8
Spatial resolution [μm]	216
Strain resolution [με]	135

In addition, a PCI-2 acoustic emission (AE) system was used to verify the onset of fragmentation in the hybrid sensors. The AE sensor acquiring the data was a PAC WSA type, broadband, piezoelectric transducer with a frequency range of 100-1000 kHz. The maximum sampling rate was 40 MHz and the gain selector of the preamplifier and threshold value were set to 40 dB. The acoustic sensors were attached to the back face of the tensile specimens (bottom side of the substrate) by using a hot melt adhesive gun. The adhesive was only applied to the side of the sensors so as not to affect the acoustic coupling. Silicone grease was used to provide sufficient coupling between the specimens and the sensor. Furthermore, each specimen was tapped by a stiff object at the start of the tests in order to provide a time reference point to the various data acquisition systems.

4.5. Results and discussion

4.5.1. Sensor trigger strain identification

Figure 6 shows the load-strain response of a typical tensile specimen fitted with a long unidirectional hybrid sensor comprising single layers of XN80 carbon/epoxy and S-glass/epoxy prepreg.

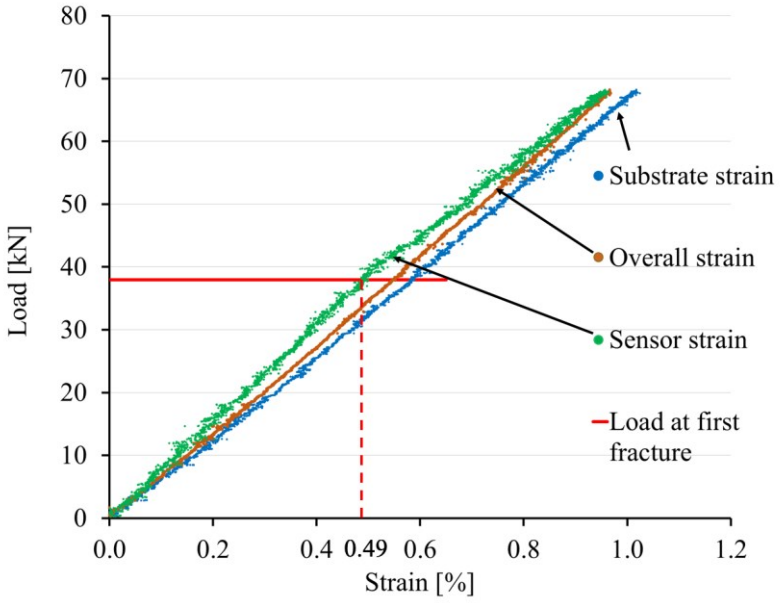

Figure 6. Typical load-strain response of a tensile specimen fitted with a co-cured, single layer XN80/epoxy UD hybrid sensor

The substrate strain (defined between points of U and V in Figure 5) represents the surface strain of the substrate only, the overall strain (defined between points of U and Z in Figure 5) represents the overall extension measured along the free length of the specimen, while the sensor strain (defined between points of X and Y in Figure 5) shows the surface strain of the sensor. The red dashed and continuous lines illustrate the strain and load respectively at which the first sensing layer fracture occurred. Stresses and strains were determined from the logged data based on visually inspecting the videos recorded during testing and extracting the time for the first visible fracture of the sensing layer. The load-strain curves of Figure 6 show how the stiffness of this specimen has been increased locally due to the integration of the sensor (difference between green and blue curves). This stiffening effect demonstrates that the trigger strain of the sensors has to be corrected for the added stiffness by the sensor to represent the strain in the free-standing substrate.

4.5.2. Experimental validation for baseline configuration

As mentioned earlier, preliminary tests have been carried out in order to investigate a range of stiffnesses (different number of carbon layers) added to the structure. The minimum stiffness (one carbon sensing layer) satisfactorily indicated the overload of the substrate material. Then, a comprehensive set of specimens were tested with the optimal configuration: co-curing a long, single XN80 ply carbon/epoxy sensor to the substrate laminate. Co-curing was chosen as the attachment method as this assures the highest integrity of the bond of the sensor to the substrate and provides the most accurate sensor response. The summary of the test results is given in Table 6.

Table 6. Summary of test results for the optimal sensor configuration

Integration method/sensor type	**No. of specimens tested**	**Overall strain (at first crack in sensor layer)**	**Sensor strain (at first crack in sensor layer)**	**Substrate strain (at first crack in sensor layer)**	**Substrate stress at first crack in sensor layer**
	[-]	**[%] (CV%)**	**[GPa] (CV%)**	**[%] (CV%)**	**[MPa] (CV rel.%)**
Co-cured/Long single ply [XN80]/SG	5	0.58 (3.9)	0.52 (3.3)	0.62 (4.6)	820 (5.2)

All the results presented are average surface strain values. For these specimens, the average apparent load per unit strain at the section where the sensor is placed (measured between points X and Y on Figure 5) is 75.60 kN / % strain while at the substrate only section it is 66.69 kN /% strain based on the initial slope of the load-strain curves. This resulted in a small mismatch between the sensor and substrate strains at trigger which can be corrected [26].

Furthermore, - in addition to the baseline configuration -, co-cured long double XN80 ply sensor specimens and retrofitted (long and short single ply type) specimens have been examined as shown in Table 7.

Table 7. Summary of test results for additional sensor configurations and integration methods

Integration method/sensor type	**No. of specimens tested**	**Overall strain at first crack in sensor layer**	**Sensor strain at first crack in sensor layer**	**Substrate stress at first crack in sensor layer**
	[-]	**[%] (CV%)**	**[GPa] (CV%)**	**[MPa] (CV rel.%)**
Co-cured/Long double ply [XN80]$_2$/SG	3	0.58 (2.4)	0.49 (3.6)	814.0 (5.3)
Retrofitted/Long single ply [XN80]/SG	4	0.57 (4.1)	0.54 (3.6)	748.1 (2.5)
Retrofitted/Short single ply [XN80]/SG	3	0.63 (4.1)	0.56 (5.9)	910 (2.1)

4.5.3. Comparison of different variants

Regarding the co-cured configurations, both the long single (Table 6) and double layer (Table 7) sensors show consistency in measured overall and sensor strains and the stress state in the substrate at the appearance of the first crack. The sensor strains measured for these specimens at the first crack appearance in the sensor layer (0.52% and 0.49% for single and double layers respectively) are close to the quoted failure strain (0.5%) of the UHM XN80 carbon fibres (see Table 1). The single XN80 ply carbon/epoxy sensor specimens exhibited slightly higher trigger strains at the first carbon failure than the ones with two layers. There are various factors that can contribute to this phenomenon. One of them is the hybrid effect [30]. In the case of a single XN80 ply sensor, the development of critical clusters is more restrained as the thickness

of the carbon ply is only of the order of a few fibre diameters, hence the formation of the first macroscopic crack may have been delayed. Another possible influence is the volume effect, whereby the smaller volume of material for a single ply sensor reduces the probability of finding defects of a certain size within the sensing layer, therefore increasing the strain at first fracture. The stiffness of the sensor in addition to that of the substrate also affects the measured strains.

When the sensing layer is thin, there is little added stiffness, and the sensor accurately measures the substrate strain. In this case, the hybrid effect may increase the failure strain of the sensor, slightly increasing the strain on the substrate at which the sensor triggers. On the other hand, when the sensing layer is thick, the hybrid effect is negligible, but the substrate strain and the strain of the sensor may differ because of the added stiffness. This potential difference in strains could decrease the accuracy of the sensors, especially in the case of thinner parts.

Regarding the retrofitted specimens, they were only equipped with single XN80 ply sensors (Table 7). The specimens with shorter sensors showed higher trigger strains as well as elevated stresses in the substrate at the first fracture of the sensing layer. This general trend, an increase in overall strain in the case of the specimens fitted with shorter sensors – is because the stress from the substrate and the glass layer was transferred to the sensing layer along the ineffective length of the layer (half ineffective length at both ends). The ineffective length is calculated to be 2.44 mm and 4.87 mm (see Table 3) for single/double XN80 ply sensing layers respectively (this is one of the reasons why there were no short double ply sensors tested). In the case of the retrofitted short, single layer sensor specimens, it means that approximately a quarter of the volume of the sensing layer is not fully loaded, hence the corresponding extra volume effect may have delayed the appearance of the first crack in the sensor slightly. Despite this, the short sensors may still be suitable for smaller components where it is not possible to

fit the longer ones but they have to be designed with special attention to the effects highlighted above and calibrated to the substrate stiffness.

4.5.4. Damage visualization and trigger strain verification

Digital Image Correlation (DIC) and Acoustic Emission (AE) measurements have been carried out to verify the time and appearance of the first fibre fracture and fragmentation occurring in the sensing carbon layers.

The strain distribution of a co-cured specimen with the optimal sensor configuration can be seen in Figure 7, where the original specimen and the area used for the analysis is shown in Figure 7 (a), while the other plots show the strain distribution before carbon layer fragmentation – Figure 7 (b)- , at first crack appearance – Figure 7 (c)-, and after well dispersed cracking and local delamination in the hybrid composite sensor- Figure 7 (d). The area used for DIC analysis only covered half the width of each specimen, as the other half was used for visual confirmation of the sensor concept as illustrated in Figure 7 (a).

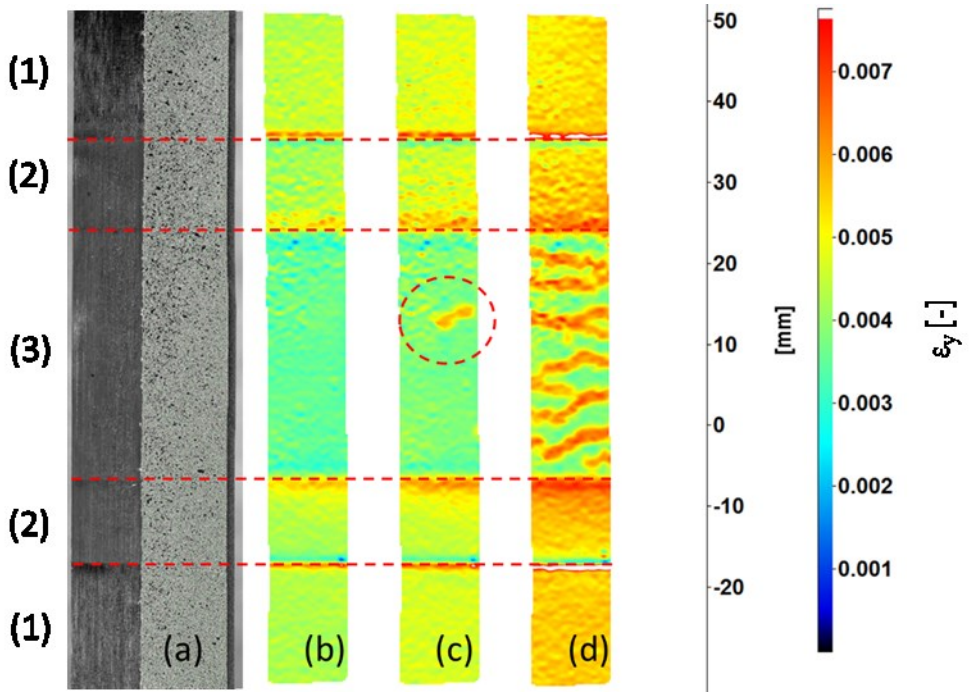

Figure 7. Longitudinal strain distribution of a co-cured specimen equipped with a single ply XN80/epoxy and S-Glass/epoxy sensor. The figure illustrates (a) the original specimen and the area used for DIC analysis, (b) the strain distribution on the surface of the specimen before carbon layer fragmentation (c) at first crack appearance in the carbon sensing layer (d) after well-dispersed cracking and local delamination occurring in the hybrid sensor laminate

The numbered regions in Figure 7 represent distinct areas of the specimens: (1) substrate only (2) substrate + glass layer and (3) substrate + glass + carbon layer. Local strain concentrations can be observed at the transitions between different material regions. In order to quantitatively assess the strain variation and more adequately resolve the strain field, a high resolution DIC measurement system should be used specifically directed at a smaller area - Region of Interest (ROI) - eg. around the sensors: region (3) on Figure 7 (a).

In order to further confirm the accuracy of how the trigger strain of the sensors is determined, the results were also compared with acoustic emission measurements on the specimens. Figure 8 illustrates the (a) acoustic emission energy and (b) cumulative acoustic energy as a function of the applied load in the case of a co-cured specimen fitted with a single XN80/epoxy ply sensor.

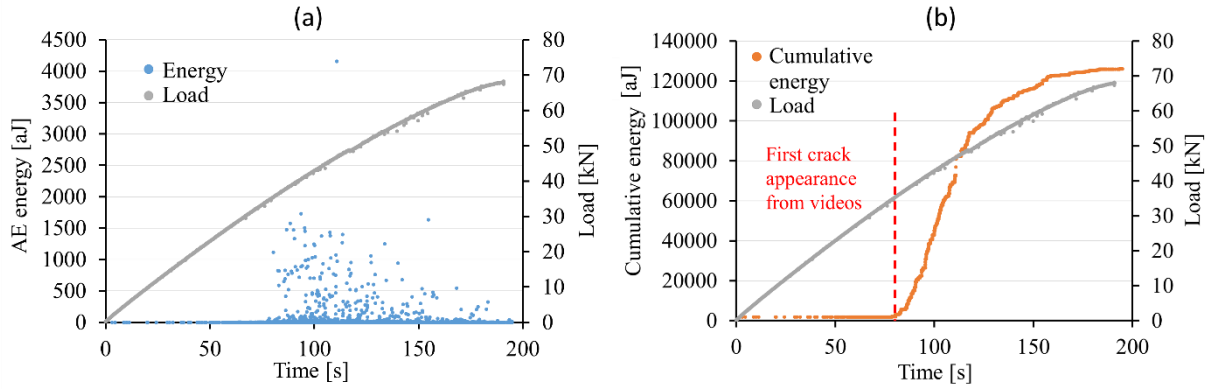

Figure 8. Typical AE results of a specimen fitted with the optimal sensor configuration: (a) acoustic emission energy and (b) cumulative energy in function of the applied uniaxial tensile load

The onset of fragmentation in the sensing carbon layer is accompanied by a significant rise in the cumulative energy, as shown in Figure 8 (b). This corresponds to the AE energy diagram where fragmentation initiates at the same time as the rise of cumulative energy. The appearance of the striped pattern and the obtained AE signals show similarities with the work carried out by Fotouhi et al. [31] who correlated the number of AE events in a UD carbon/S-glass hybrid laminate with direct observations of fragmentation during the loading of the specimens.

According to Figure 8 (a), the onset of fragmentation from the AE starting at t = 84.69 s matches the appearance of the first crack in the carbon sensing layer observed and extracted from the recorded videos (t = 84.81 s).

4.5.5. Comparison of adhesives for retrofitted specimens

A brief study was carried out to determine the ease and quality of the different bonding methods. It was concluded that the Araldite two-part epoxy adhesive, the MBond AE15 high strain strain gauge epoxy adhesive and the Hexcel 913 resin film provided sufficient bonding when attaching sensors to the composite substrates. For these adhesives, all the sensors

exhibited the expected striped pattern without any premature debonding. Overall, it can be said that the Araldite epoxy system was the easiest and most cost efficient to apply to a substrate/component, however the more expensive high strain MBond epoxy adhesive exhibited the best surface quality finish due to its translucent nature and low viscosity. The cyanoacrylate adhesive did not provide sufficient bonding between the sensor and the substrate material as the sensor delaminated during uniaxial tensile testing.

4.6. Application case study

In order to demonstrate the overload sensor concept, single ply XN80/epoxy short and long hybrid composite sensors were integrated on a commercially available carbon fibre reinforced polymer (CFRP) bike handlebar. The 3T Flat 720 Team Stealth mountain bike (MTB) mount flat bar was retrofitted with both long and short type sensors and a three-point bending test was carried out on the structure. The same test in a similar set-up was repeated for a handlebar without any sensors attached to it.

Due to the curved geometry of the components' surface the sensors had to be pre-curved in the appropriate direction (longitudinally or transversely to the fibres) according to the loading conditions of the application. The sensor laminates were laid up onto an aluminium tube that was surface treated by a release agent (Loctite Freekote 700 NC). An envelope bagging process was applied on a hollow aluminium tool before autoclave curing. The same diameter tooling was chosen, matching the curvature of the bike handlebars.

For the retrofitting of these curved sensors, an Araldite 2014/1 type epoxy system has been utilised in a similar way to applying strain gauges for composite materials [32]. Additionally, to ensure a good surface quality and void free bonding, vacuum assisted envelope bagging was used when curing the adhesive in an atmospheric oven at 80 °C for 2hrs.

The force-displacement curves of the tested MTB handlebars can be seen in Figure 9.

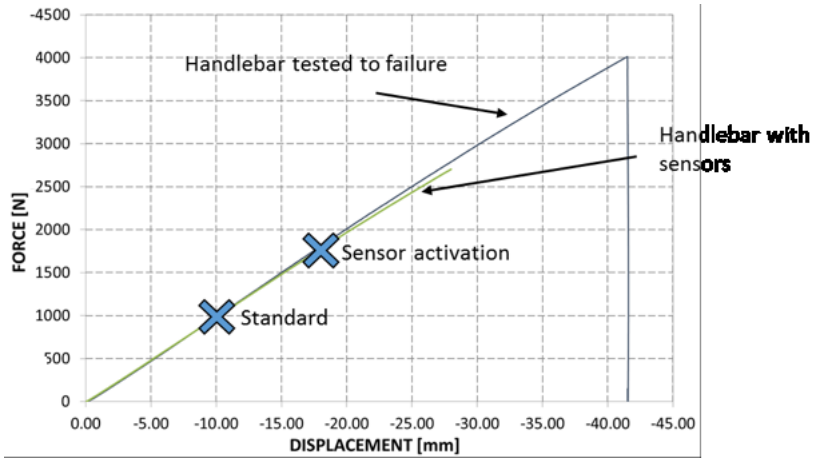

Figure 9. Force-displacement curves of the tested CFRP bike handlebars

The graph highlights the point at which the long sensors activated as well as marking the load (1000 N) that generally applies for the testing of Racing Bicycle handlebars according to the European Standard (EN14781) [33].

Whilst the shorter sensors did not trigger for the applied load of 2700N, the first carbon layer fracture of the long sensors - visualizing the overload of the bar - was observed at 1750 N. It is worth noting that there was no stiffness increase observed on the force-displacement graphs indicating that the attached sensors did not make a significant difference to the loading of the tested handlebar. The illustration of the handlebar with various sensors integrated to it can be seen in Figure 10. Overall, it can be said that the long sensors applied to the bike handlebar performed well in demonstrating the sensor concept and providing a warning to the user that an overload event had occurred.

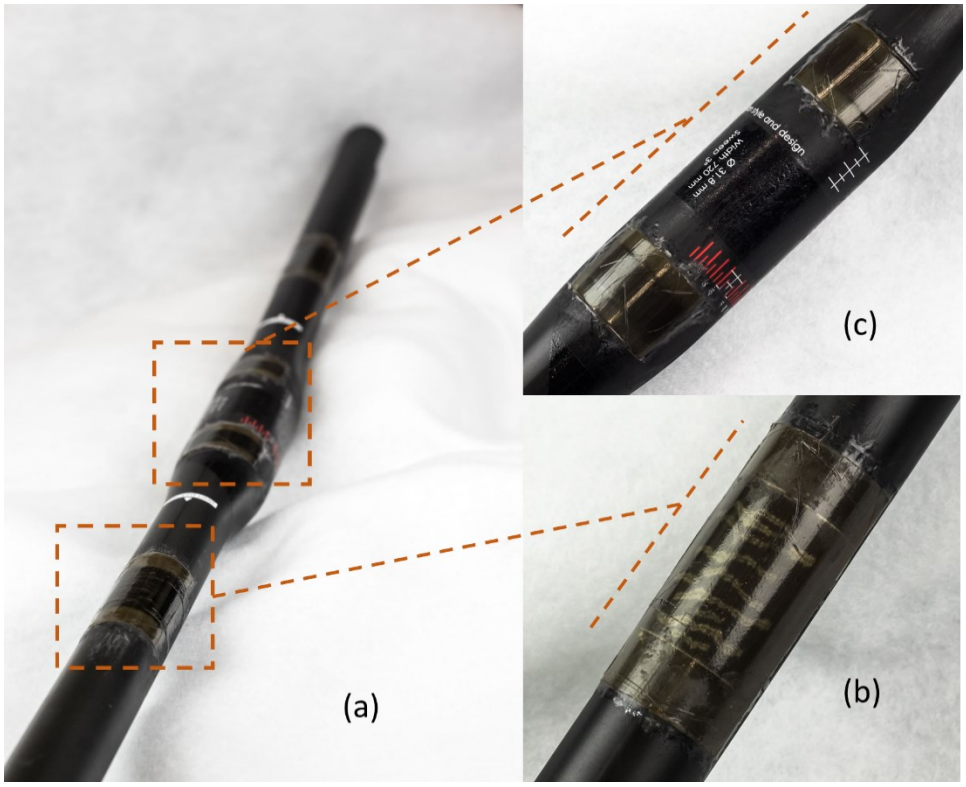

Figure 10. Bike handlebar fitted with hybrid composite overload sensors: (a) MTB Racing flat handlebar, retrofitted with (b) long single layer (c) short single layer sensors

5. Conclusions

A novel Structural Health Monitoring (SHM) concept has been proposed that visually indicates the strain overload of a structure. The unidirectional (UD) hybrid composite sensors clearly exhibit a change in appearance when loaded over a predefined strain value. These purpose-designed composite sensors are lightweight, robust and completely wireless, hence it is a very promising technology in advanced safety-critical applications especially in the fields of sporting goods, civil engineering or pressure vessels.

They are highly tailorable as (i) they can be embedded or locally integrated to the structure, (ii) they can be designed for the desired application both in terms of the magnitude and direction of overload strain (applicable strain range: 0.3%-2%) and (iii) they can be designed for different substrate materials (including metals and composites). The most important influencing parameters of such sensors are the ineffective length and stiffness of the

sensing layer relative to the stiffness of the substrate material. The sensor has to be designed for the substrate material/component for optimum performance.

An overall increase in the trigger strain was found for the shorter length sensors rendering them less accurate for overload strain indication. This is because a significant part of the short sensing layer was inactive (one quarter of the sensing length in case of the short single ply sensors). Therefore, it is recommended to use a sensor layer length of at least 5 times the critical length. An optimal configuration was found incorporating long single plies of XN80/epoxy and S-glass/epoxy material (30 mm for the sensing- and 50 mm for the translucent layer). The proof of concept of the presented hybrid composite sensors has been successfully demonstrated through mechanical characterisation and the integration of such sensors to a real-life application demonstrator: a CFRP bicycle handlebar.

Acknowledgements

This work was funded under the UK Engineering and Physical Sciences Research Council (EPSRC) Programme Grant EP/I02946X/1 on High Performance Ductile Composite Technology in collaboration with Imperial College London. Tamas Rev would like to acknowledge the EPSRC Centre for Doctoral Training in Advanced Composites for Innovation and Science at the Bristol Composites Institute. Gergely Czél acknowledges the Hungarian National Research, Development and Innovation Office (NKFIH) for funding through grants ref. OTKA K 116070, OTKA PD 121121 and NVKP_16-1-2016-0046, the Hungarian Academy of Sciences for funding through the János Bolyai scholarship and the Hungarian Ministry of Human Capacities (EMMI) for funding through the BME-Nanonotechnology FIKP grant (BME FIKP-NAT). The authors would like to acknowledge Hexcel Corporation and North TPT for supplying the materials for this research. The data required to support the conclusions are provided within the paper.

6. References

[1] Zweben C. Advanced composites for aerospace applications - A review of current status and future prospects. Composites 1981;12:235–40.

[2] Selman E, Ghiami A, Alver N. Study of fracture evolution in FRP-strengthened reinforced concrete beam under cyclic load by acoustic emission technique: An integrated mechanical-acoustic energy approach. Constr Build Mater 2015;95:832–41.

[3] Gay D, Hoa S V., Tsai SW. Composite materials: Design and Applications. London: CRC Press; 2003.

[4] Swolfs Y, Verpoest I, Gorbatikh L. Recent advances in fibre-hybrid composites : materials selection , opportunities and applications. Int Mater Rev 2018:1–35.

[5] Maleque MA, Salit MS. Materials Selection and Design. London: Springer; 2013.

[6] Czél G, Jalalvand M, Wisnom MR. Design and characterisation of advanced pseudo-ductile unidirectional thin-ply carbon/epoxy– glass/epoxy hybrid composites. Compos Struct 2016;143:362–70.

[7] Jalalvand M, Czél G, Wisnom MR. Parametric study of failure mechanisms and optimal configurations of pseudo-ductile thin-ply UD hybrid composites. Compos Part A Appl Sci Manuf 2015;74:123–31.

[8] Czél G, Wisnom MR. Demonstration of pseudo-ductility in high performance glass/epoxy composites by hybridisation with thin-ply carbon prepreg. Compos Part A Appl Sci Manuf 2013;52:23–30.

[9] Amafabia DM, Montalvão D, David-West O, Haritos G. A Review of Structural Health Monitoring Techniques as Applied to Composite Structures. Struct Durab Heal Monit 2017;11:91–147.

[10] Rana S, P S, Fangueiro R, Gomes Correia A. A review on smart self-sensing composite materials for civil engineering applications. AIMS Mater Sci 2016;3:357–79.

[11] Ciang CC, Lee J-R, Bang H-J. Structural health monitoring for a wind turbine system: a review of damage detection methods. Meas Sci Technol 2008;19:122001.

[12] Kinet D, Mégret P, Goossen KW, Qiu L, Heider D, Caucheteur C. Fiber Bragg grating sensors toward structural health monitoring in composite materials: challenges and solutions. Sensors 2014;14:7394–419.

[13] Ye XW, Su YH, Han JP. Structural Health Monitoring of Civil Infrastructure Using Optical Fiber Sensing Technology: A Comprehensive Review. Sci World J 2014;2014:652329.

[14] Alexopoulos ND, Bartholome C, Poulin P, Marioli-Riga Z. Structural health monitoring of glass fiber reinforced composites using embedded carbon nanotube (CNT) fibers. Compos Sci Technol 2010;70:260–71.

[15] Todoroki A, Tanaka M, Shimamura Y. Electrical resistance change method for monitoring delaminations of CFRP laminates: Effect of spacing between electrodes. Compos Sci Technol 2005;65:37–46.

[16] Todoroki A, Omagari K, Shimamura Y, Kobayashi H. Matrix crack detection of CFRP using electrical resistance change with integrated surface probes. Compos Sci Technol 2006;66:1539–45.

[17] Abry J. In situ detection of damage in CFRP laminates by electrical resistance measurements. Compos Sci Technol 1999;59:925–35.

[18] Song DY, Takeda N, Kitano A. Correlation between mechanical damage behavior and electrical resistance change in CFRP composites as a health monitoring sensor. Mater Sci Eng A 2007;456:286–91.

[19] Pissis P, Georgousis G, Pandis C, Georgiopoulos P, Kyritsis A, Kontou E, et al. Strain and Damage Sensing in Polymer Composites and Nanocomposites with Conducting Fillers. Procedia Eng 2015;114:590–7.

[20] Kwon DJ, Wang ZJ, Choi JY, Shin PS, Devries KL, Park JM. Damage sensing and fracture detection of CNT paste using electrical resistance measurements. Compos Part B Eng 2016;90:386–91.

[21] Obitayo W, Liu T. A review: Carbon nanotube-based piezoresistive strain sensors. J Sensors 2012;2012.

[22] Park J-M, Kwon D-J, Wang Z-J, DeVries KL. Review of self-sensing of damage and interfacial evaluation using electrical resistance measurements in nano/micro carbon materials-reinforced composites. Adv Compos Mater 2015;24:197–219.

[23] Czél G, Jalalvand M, Potter K, Wisnom MR. UK Patent Application number: 1520988.5, n.d.

[24] Bakis CE, Nanni A, Terosky JA, Koehler SW. Self-monitoring, pseudo-ductile, hybrid FRP reinforcement rods for concrete applications. Compos Sci Technol 2001;61:815–23.

[25] Nanni F, Ruscito G, Forte G, Gusmano G. Design, manufacture and testing of self-sensing carbon fibre–glass fibre reinforced polymer rods. Smart Mater Struct 2007;16:2368–74.

[26] Rev T, Czél G, Jalalvand M, Wisnom MR. Unidirectional hybrid composite overload sensors – robust tools for visual overload indication. ICCM21', vol. 1, Xi'an, China: 2017.

[27] Czél G, Jalalvand M, Wisnom MR. Hybrid specimens eliminating stress concentrations in tensile and compressive testing of unidirectional composites. Compos Part A Appl Sci Manuf 2016;91:436–47.

[28] Czél G, Jalalvand M, Wisnom MR. Demonstration of pseudo-ductility in unidirectional hybrid composites made of discontinuous carbon/epoxy and continuous glass/epoxy plies. Compos Part A Appl Sci Manuf 2015;72:75–84.

[29] Wisnom MR, Jones MI. Size effects in interlaminar tensile and shear strength of unidirectional glass fibre/epoxy. J Reinf Plast Compos 1996;15:2–15.

[30] Wisnom MR, Czél G, Swolfs Y, Jalalvand M, Gorbatikh L, Verpoest I. Hybrid effects in thin ply carbon/glass unidirectional laminates: Accurate experimental determination and prediction. Compos Part A Appl Sci Manuf 2016;88:131–9.

[31] Fotouhi M, Suwarta P, Jalalvand M, Czel G, Wisnom MR. Detection of fibre fracture and ply fragmentation in thin-ply UD carbon/glass hybrid laminates using acoustic emission. Compos Part A Appl Sci Manuf 2016;86:66–76.

[32] Vishay Micro-measurements Application Note VMM-19. Surface Preparation of Composites n.d.:11183.

[33] CEN. Racing bicycles - Safety requirements and test methods (EN 14781) 2005:80.